High-Nonlinearity Dispersion-Shifted Lead-Silicate Holey Fibers for Efficient 1-μm Pumped Supercontinuum Generation

J. Y. Y. Leong, P. Petropoulos, J. H. V. Price, Heike Ebendorff-Heidepriem, S. Asimakis, R. C. Moore, K. E. Frampton, V. Finazzi, X. Feng, T. M. Monro, and D. J. Richardson

***Abstract*—This paper reports on the recent progress in the design and fabrication of high-nonlinearity lead-silicate holey fibers (HFs). First, the fabrication of a fiber designed to offer close to the maximum possible nonlinearity per unit length in this glass type is described. A value of $\gamma = 1860\ \mathrm{W}^{-1} \cdot \mathrm{km}^{-1}$ at a wavelength of 1.55 μm is achieved, which is believed to be a record for any fiber at this wavelength. Second, the design and fabrication of a fiber with a slightly reduced nonlinearity but with dispersion-shifted characteristics tailored to enhance broadband supercontinuum (SC) generation when pumped at a wavelength of 1.06 μm—a wavelength readily generated using Yb-doped fiber lasers—are described. SC generation spanning more than 1000 nm is observed for modest pulse energies of $\sim$ 100 pJ using a short length of this fiber. Finally, the results of numerical simulations of the SC process in the proposed fibers are presented, which are in good agreement with the experimental observations and highlight the importance of accurate control of the zero-dispersion wavelength (ZDW) when optimizing such fibers for SC performance.**

***Index Terms*—Holey-fibers (HFs), optical fiber fabrication, photonic crystal fibers (PCFs).**

I. Introduction

THE ADVENT of holey-fiber (HF) technology has enabled the design and fabrication of optical fibers with unique and enabling optical properties, opening a host of new scientific and technological opportunities. These unique optical properties, for example, endlessly single mode guidance [1], result directly from the way that the guided mode "experiences" the microstructured cladding region. In a conventional fiber, this is, to the first order, independent of wavelength. However, in an HF, the large index contrast between glass and air and the small structural dimensions combine to make the effective cladding index strongly wavelength dependent. Moreover, the large index contrast itself allows for more extreme values of numerical aperture (NA), which can be achieved using conventional doped fiber technology. The structural design space for HFs is also very rich, and these factors combined ensure that HFs can have a substantially broader range of optical properties than conventional optical fibers.

Arguably, one of the most exciting prospects for microstructured fiber technology is the development of fibers with large values of optical nonlinearity per unit length $\gamma = 2\pi n_2/\lambda A_{\mathrm{eff}}$, where n_2 is the Kerr nonlinear coefficient for the glass and A_{eff} is the effective area. Fibers with a small core dimension and a cladding with a large air-fill fraction allow for extremely tight mode confinement, i.e., small effective area, and hence, a high value of γ [2]. Using this approach, it has been possible to fabricate pure-silica HFs with a γ of 70 $\mathrm{W}^{-1} \cdot \mathrm{km}^{-1}$ at 1.55 μm (note, for comparison, that the corresponding value for conventional single-mode fibers is $\sim 1\ \mathrm{W}^{-1} \cdot \mathrm{km}^{-1}$) [3]. This is close to the ultimate limit that can be achieved in silica, restricted by the nonlinear refractive index n_2 of this glass and minimum achievable effective area [4].

Significantly higher values of γ can be achieved by combining tight mode confinement with the use of glasses with greater intrinsic material nonlinearity coefficients than silica. Examples of suitable glasses that have been used to make HFs include chalcogenide [5], tellurite [6], [7], bismuth oxide [8], and lead-silicate glasses [9]–[12]. The emergence of HF technology is particularly enabling in terms of making fibers in these more exotic glasses since it allows fibers to be made from just a single material, eliminating the need for two thermally, chemically, and optically compatible glasses to form the fiber core and cladding. Compound glasses also exhibit far lower processing temperatures than silica (for example, each of the above glasses exhibits low softening temperatures of $\sim 500\ ^{\circ}\mathrm{C}$, as opposed to $\sim 2000\ ^{\circ}\mathrm{C}$ for silica), which enable the use of extrusion for fiber preform manufacture. Aside from being simpler and less labor intensive than the more conventional stacking technique developed for silica HFs, extrusion readily allows the implementation of structures with high-air-content claddings, as required for high-nonlinearity HF fabrication. Of all the aforementioned high-index glass types, lead-silicate glasses offer the good thermal and crystallization stability, and exhibit the relatively flat viscosity–temperature curves, making them particularly attractive for microstructured fiber fabrication, although the fact that their intrinsic material nonlinearity is lower than that of chalcogenide and heavy metal oxide glasses is also to be appreciated [13]. Schott SF57, which is

Manuscript received July 14, 2005; revised October 5, 2005. The works of J. Y. Y. Leong and S. Asimakis were supported by the Malaysian Government Studentship and by the Greek State Scholarships Foundation, respectively.

J. Y. Y. Leong, P. Petropoulos, J. H. V. Price, S. Asimakis, R. C. Moore, K. E. Frampton, V. Finazzi, X. Feng, and D. J. Richardson are with the Optoelectronics Research Centre, University of Southampton, Southampton, U.K. (e-mail: jyyl@orc.soton.ac.uk).

H. Ebendorff-Heidepriem and T. M. Monro were with the Optoelectronics Research Centre, University of Southampton, Southampton, U.K. They are now with The School of Chemistry and Physics, University of Adelaide, Adelaide, Australia.

Digital Object Identifier 10.1109/JLT.2005.861114

the glass on which we have focused in this work, exhibits the highest nonlinearity among the commercially available lead-silicate glasses. The high lead concentration of this glass leads to the large linear refractive index of 1.81 at 1.55 μm and large nonlinear refractive index of 4.1×10^{-19} m^2/W (as measured at 1.06 μm [14]). Although much higher than silica, losses in bulk SF57 can be as low as 0.3 dB/m at 1.55 μm [14].

For most nonlinear fiber applications, control of the fiber dispersion is more important than achieving the maximum possible nonlinearity per unit length, and here, again, the use of HF technology provides unique opportunities. The small core dimensions possible in HFs with a high cladding air-fill fraction result in a strong wavelength dependence of the effective cladding index, which affects both the magnitude and spectral profile of the waveguide dispersion. This can be used to control the total fiber dispersion over extended wavelength ranges compared to conventional solid fibers. For example, in silica-glass HFs, it is possible to achieve anomalous dispersion at visible wavelengths, i.e., at wavelengths much shorter than the material zero-dispersion wavelength (ZDW), allowing soliton formation at wavelengths shorter than 600 nm [15]. Similar benefits in terms of controlling the dispersion properties of fibers at wavelengths of technological interest can be obtained in compound-glass HFs. The material ZDW for SF57 glass is ~ 1.97 μm; yet, as we show in this paper, it is possible to use the large waveguide dispersion available in SF57 HFs to obtain fibers with ZDWs shifted by more than 1000 nm to allow efficient SC generation when pumped at wavelengths around 1 μm. SC generation depends on the fiber characteristics over a broad range of wavelengths, so complex dispersion profiles—for example, with two ZDWs—could also be envisaged, as suggested by other authors [16]. For this initial experimental demonstration, we have considered a single ZDW, and this has practical significance as it reduces the pulse energies required for the initial stages of SC generation down to the 100-pJ regime—a pulse-energy regime that can readily be accessed directly from mode-locked Yb-doped fiber laser cavities. This should lead to the development of truly compact and practical SC sources for metrological applications. To date, the majority of work on SC generation has used nanojoule pulses from bulky and expensive Ti–Sapphire laser systems, which has restricted widespread deployment of the technology.

The objective of this work is to explore the limits of nonlinearity and dispersion control in lead-silicate-based microstructured fibers. Our focus has been on establishing the maximum nonlinearity that can be achieved in these fibers at telecommunications wavelengths and to develop high-nonlinearity fibers with dispersion-shifted characteristics suited for SC-generation applications at 1.06 μm. The paper is organized as follows. The next section describes the results of a systematic study of how our fiber design parameters affect the fiber nonlinearity dispersion and mode profile. In Section III, we describe the results of our work on the fabrication and characterization of fibers, both with record nonlinearity at 1550 nm, and high-nonlinearity fibers with a ZDW shifted to the 1-μm regime. The rest of the paper is devoted to the SC studies we carried out using the two types of fibers produced. We present both experiments and numerical simulations and discuss how the properties of each of the fibers affected the broadened spectra. The conclusions of this work are presented in Section V.

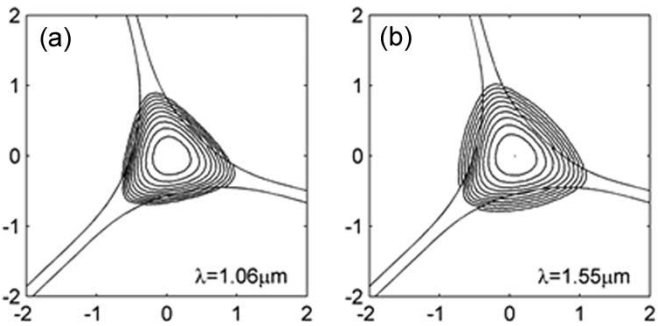

Fig. 1. Predicted mode intensity profiles for HF of core diameter ~ 0.95 μm (Fiber#1) at (a) 1.06 μm and (b) 1.55 μm (1 dB per contour).

II. Fiber Design and Modeling

Before starting any fabrication work, we performed an initial assessment of how the nonlinear and dispersive properties of high-nonlinearity lead-silicate fibers vary with core structure. We assumed a similar geometric fiber design to that adopted in our earlier work in SF57 [9], [11] and bismuth-oxide HFs [8]. According to this design, which is readily achieved through a two-step preform extrusion technique, a small core is supported by three fine and long struts (see Figs. 1 and 4), which ensures a very large air-fill fraction in the surrounding cladding region, and high optical isolation between the core and the glass in the jacket of the fiber. This high-NA design closely resembles the air-suspended rod (ASR) structure—an idealized configuration of a circular glass core surrounded by air. Consequently, we used an ASR model in our initial studies to help us establish the range of core dimensions that we should target in our initial fabrication attempts to realize high-nonlinearity dispersion-shifted fibers. It is however to be appreciated that our three-strut design, which naturally results in a triangular-shaped core, gives slightly increased values of A_{eff}, and increased confinement losses compared to an ASR of the same geometric area. Therefore, in order to refine our findings, we repeated our calculations after fiber fabrication using scanning electron microscopy (SEM) images of the actual fibers fabricated. It is the results of these refined calculations on real structures that are presented in this section.

For our calculations, we first studied the modal characteristics of the HF waveguide. Single transverse-mode operation is a prerequisite for most applications. However, because of the extremely high NA of these HFs, single-mode operation is not always rigorously obtained. Nevertheless, many HFs can be effectively single mode over a broad range of wavelengths since the confinement losses associated with any higher order modes supported theoretically by the structure are significantly higher than those of the fundamental mode. For our specific design, single-mode operation can be achieved when reducing the scale of the microstructure beyond a certain value. Practically, for this type of HF, single-mode or effectively single mode operation was obtained for a core diameter of 1.8 μm or less at 1.047 μm (Nd:YLF laser). Note that when specifying core diameters for

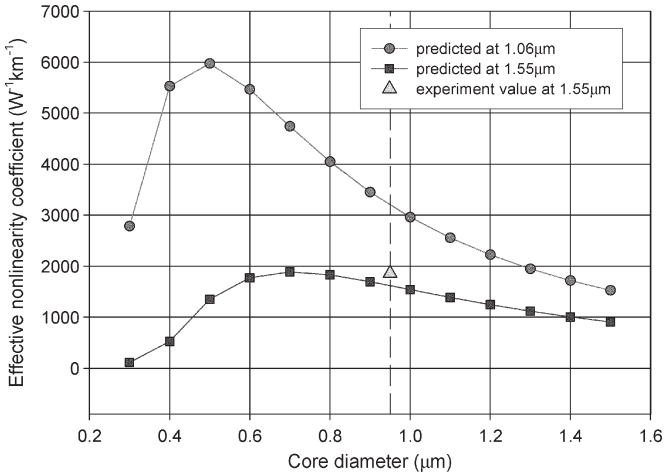

Fig. 2. Effective nonlinear coefficient at 1.55 and 1.06 μm.

our fibers, we are referring to the diameter of the circle that just fits within the triangular-core region, as illustrated in Fig. 4(a). The fundamental modes of our fibers reflect the triangular symmetry of the fiber core, as illustrated in Fig. 1, where we plot the theoretical fundamental mode profiles at wavelengths of both 1 and 1.55 μm for a fiber with an ~ 0.95-μm core diameter. These calculations were performed using a commercial beam propagation package based on a core geometry as extracted from an SEM image of the fiber. For both wavelengths, the predicted profile of the guided mode has a triangular shape. The predicted effective mode areas are 0.84 μm^2 at 1.06 μm and 1.1 μm^2 at 1.55 μm.

Fig. 2 shows a prediction of the effective nonlinearity γ of an SF57 HF as a function of the core diameter calculated at 1.06 and 1.55 μm. These calculations were performed using a commercial full-vector modal solver, based on the finite element method (FEM). The figure shows that the effective nonlinearity can be drastically enhanced by decreasing the core diameter due to the tighter mode confinement. The nonlinearity increases up to the point that the core becomes too small to confine the mode tightly. For diameters below this critical diameter, the effective nonlinearity decreases rapidly as the mode spreads progressively further out of the core and into the air. The ultimate limit on fiber nonlinearity at 1.55 μm is nearly 2000 W$^{-1}\cdot$ km^{-1} for triangular-core HFs with core diameters in the range 0.6–1.0 μm. It should be noted that higher values of effective nonlinearity can be achieved at shorter wavelengths due to a combination of the $1/\lambda$ wavelength of γ and the fact that shorter wavelengths can be confined to the core down to smaller core dimensions.

In order to assess the dependence of the fiber-dispersion characteristics on the HF core diameter, we evaluated the group velocity dispersion of a range of HFs with different core dimensions using an FEM code adopting the refractive index profile of the real fiber. The results of our calculations are summarized in Fig. 3, where we plot the corresponding dispersion curves for different core diameters. The waveguide dispersion is seen to have a more pronounced effect on the shape of the overall fiber-dispersion curve as the core dimension is reduced. The plots show that a fiber with a core diameter of ~ 1.3 μm results

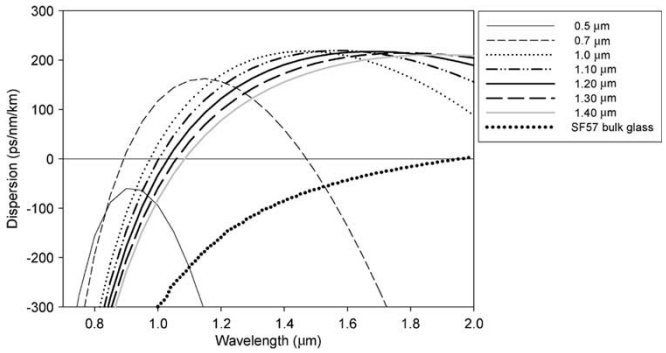

Fig. 3. Dispersion curves for bulk glass and HFs with different core diameters.

in a ZDW at 1.06 μm (note, however, that the dispersion slope is still quite high at this wavelength, i.e., ~ 1 ps/nm$^2\cdot$ km). From Fig. 2, it is seen that this fiber exhibits $\gamma = \sim 2000$ W$^{-1}\cdot$ km^{-1} at this wavelength, a factor of 3 or so less than the maximum possible nonlinearity achievable with such fibers at this wavelength. HFs with diameters around 1.3 μm thus appear well suited for nonlinear fiber-optic applications such as SC generation around 1 μm, where the combination of high effective nonlinearity and low values of chromatic dispersion are essential to realize power-efficient nonlinear devices.

III. Fiber Fabrication, Structure, and Basic Properties

The three-step procedure we use for the fabrication of our compound-glass small-core HFs has been previously reported in [8], [9], [11], and [12] and consists of 1) two extrusion procedures for the fabrication of preform elements (core preform and an outer jacket tube); 2) caning of the core preform; and finally, 3) drawing of the assembled preform into fiber. Microstructured preforms, tubes, and canes can be reliably and reproducibly fabricated in this way, and good dimensional control can be achieved. Careful adjustment of the tension applied during fiber drawing allows us to accurately control the outer diameter of the fiber, and hence, the dimensions of the inner core itself. HFs with core diameters in the range of 0.9–1.8 μm were produced from two different assemblies. From a single preform of length of $\sim$ 15 cm, we produced fiber lengths of more than 200 m, wound on a spool in several bands of uniform outer diameter in the range 100–150 μm. Note that the ratio between core size and fiber diameter can be changed via the choice of jacketing geometry and corresponding cane size, which allows the fiber diameter for a certain core size to be set to the desired value. The geometry of the microstructure can be well maintained throughout the various scale-reduction processes in going from structured preform down to the end fiber. To explore the impact of the microstructure on the fiber loss, we also drew unstructured and unclad fibers (so-called bare fibers) from extruded rods made from the same batch of SF57 material used to produce our HFs.

A typical SEM image of the resulting fiber cross section, and a magnified central region of the fiber are shown in Fig. 4(a). The three fine struts that join the core to the outer section of the fiber have a length in the range of 3–5 μm (depending on

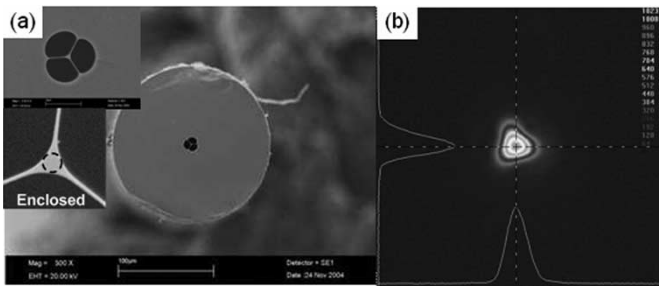

Fig. 4. (a) SEM image of the small-core extruded SF57 HF with an ~ 0.95-μm core and the enclosed area is the diameter of the circle that fits just inside the core region. (b) Measured mode profile for HF at 1.047 μm.

the core size and hole shapes) and a thickness of < 250 nm. This HF design allows the formation of extremely small cores (0.9–1.3 μm in this case) with low confinement loss (calculated to be $< 10^{-4}$ dB/m) and which provide single-mode guidance at infrared wavelengths. All of the HFs we fabricated from the two assemblies demonstrate similar transverse refractive index profiles. Note that the diameter variation along 1-m-long fiber samples used in the experiments described below was relatively small $(< \pm 0.1\ \mu\text{m})$, meaning that the dispersive properties were highly uniform along the full device length.

We have studied closely the properties and SC-generation performance of two HFs with core diameters of 0.95 ± 0.05 and 1.30 ± 0.05 μm (denoted Fiber#1 and Fiber#2, respectively). The spatial-mode guidance characteristics of Fiber#1 and Fiber#2 at 1.047 μm (Nd:YLF laser) were first investigated by imaging the near field of the guiding mode from the output end of the HF onto an infrared charge-coupled device (CCD) camera. At this wavelength, the measured fundamental mode profile for both fibers has a triangular shape [Fig. 4(b)], which is in good agreement with the predicted mode profile (Fig. 1). It can be concluded that robust single-mode guidance is observed for both fibers at 1.047 μm and, consequently, for all wavelengths longer than 1.047 μm.

The propagation loss of both fibers ($\sim$ 4 m) was then measured using the cut-back method. A tungsten halogen lamp and an optical spectrum analyzer were used to record the transmission spectra and to evaluate the loss from 350 to 1750 nm. The loss measurement of Fiber#2 is summarized in Fig. 5, where it is seen that this fiber exhibits a loss of 2.1 dB/m at 1.06 μm and 2.3 dB/m at 1.55 μm. A similar spectral loss profile was also obtained for Fiber#1, albeit with an ~ 0.2-dB/m higher loss due to the smaller core. The losses of these HF represent a significant improvement on the loss values we achieved in our first demonstration of these forms of fiber ($\sim$ 9 dB/m [11]). We attribute this to improvements in the (ultrasonic) cleaning of our preform elements. We next measured the losses of the extruded bare fiber. For this heavily multimode solid SF57 fiber, we measured a loss of 1.0 dB/m at 1 μm (Fig. 5), indicating a relatively modest increase in the background loss in going from bulk glass conventional multimode fiber to HF. This is likely to be due to surface imperfections within the structured preform, which are sampled by the mode at the air/glass boundaries of the core (see the calculated mode profiles overlaid on the fiber structure in Fig. 1). We consider that there is considerable potential for reducing further the fiber-

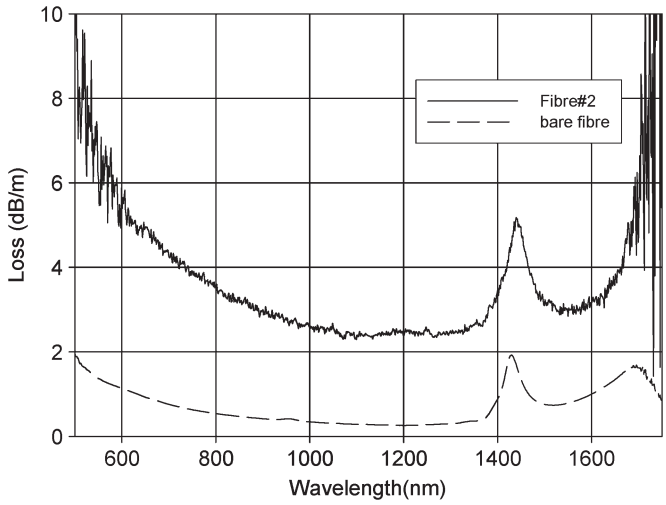

Fig. 5. White-light loss measurement of HF and bare fiber. The cut-back length used was ~ 4 m for each measurement.

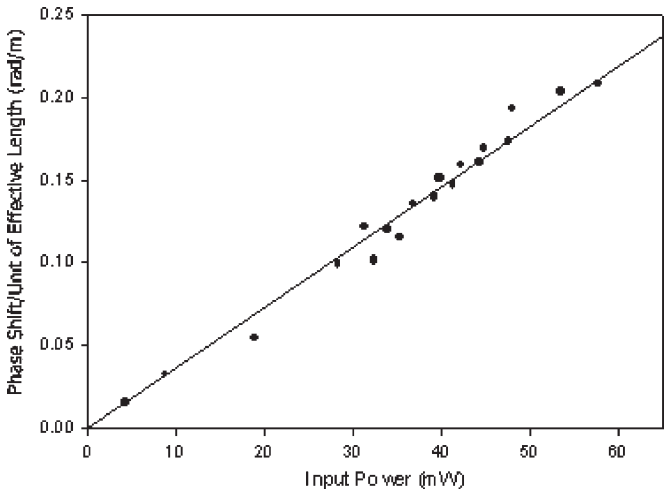

Fig. 6. Measurement of the nonlinear phase shift as a function of input power yielding $\gamma = 1860\ \text{W}^{-1} \cdot \text{km}^{-1}$ from the slope of the linear fit for Fiber#1 of length 144 cm.

loss levels in due course. Note that HF losses of 0.4 dB/m have recently been demonstrated for a small-core compound-glass HF [7].

We next estimated the effective nonlinear coefficient and effective mode area of Fiber#1 at 1.55 μm from a measurement based on the nonlinear phase induced through self-phase modulation (SPM) of a continuous-wave dual-frequency optical beat signal propagated through the fiber [16]. From the slope of the linear fit of the measurement of nonlinear phase shift versus launched power, and taking into account the effective length of the test HF (Fig. 6), we estimate a γ value of $1860\ \text{W}^{-1} \cdot \text{km}^{-1}$, which, to the best of our knowledge, is the highest nonlinearity value ever reported for an optical fiber at this wavelength. This number is, in fact, slightly higher ($\sim 10\%$) than we anticipated theoretically (Fig. 2), and we estimate it to be within $\sim 10\%$ of the maximum value possible in this glass.

The performance of a nonlinear device depends both on the effective nonlinearity and the effective length of the fiber [8]. The latter is determined by the fiber propagation loss. Although

the soft-glass HFs we present herein have much higher losses than state-of-the-art silica-based highly nonlinear fibers, their effective nonlinearity is also much higher (by almost two orders of magnitude). It follows that the required fiber length to implement a nonlinear device for practical power levels can thus be reduced considerably relative to high-nonlinearity silica fibers. Therefore, the real potential of compound-glass HFs is for the realization of short-length nonlinear devices operating at low power levels. The use of a short fiber length is significant in that it offers several important performance benefits including reduced sensitivity to external perturbations, reduced susceptibility to dispersion variation along the device length, and reduced device latency, as required, e.g., in devices such as all-optical demultiplexers, clock recovery systems, and logic gates.

IV. SC Generation

In this section, we describe our SC studies at 1.06 μm using the two SF57 HFs described above (Fiber#1 and Fiber#2). We first present our SC-generation experiments, which yielded spectra spanning over one octave and extending into the visible regions of the spectrum. We next describe a numerical model that we have used to simulate the nonlinear behavior of the fibers. Finally, the results of the simulations are compared with our experimental results. We also consider simulation results for fibers with different core sizes and conclude by suggesting promising combinations of pump wavelengths and fiber designs for continuum applications using SF57 microstructured fiber.

A. Experiments

At present, we have no ready way to measure the dispersion profile of short lengths of our fibers around 1 μm, so we rely on our spectral-broadening/SC experiments to confirm that these HFs have a low dispersion in the 1-μm range. For our SC-generation experiments, we used a diode-pumped mode-locked Nd:glass laser operating at 1.06 μm as a pump source. This laser generated 300-fs transform-limited pulses at a repetition rate of 80 MHz, and we were able to launch pulses with energies of up to $\sim$ 250 pJ into short lengths of the two fibers. Typical measured launch efficiencies into the fundamental mode were 15%–20% for these experiments, depending on the specific fiber/coupling lens choice.

The pulses were first launched into $\sim$ 60 cm of Fiber#1 ($\sim$ 0.95-μm core). Fig. 7 illustrates the spectra obtained at various launched powers. For modest power levels (launched pulse energies below $\sim$ 20 pJ), we saw clear evidence of Raman soliton formation, an indication that this HF has anomalous dispersion at the wavelength of operation. However, the presence of four-wave mixing and the generation of new components at shorter wavelengths relative to the pump is an indication that the ZDW is close to the predicted wavelengths. As we increased the power further, the spectral extent of the newly generated frequencies became broader (extended mainly towards the longer wavelength side) and the spectrum became smoother. At higher pulse energies ($\sim$ 100 pJ), the spectral components in the HF spanned more than one octave and extended significantly into the near-IR/visible wavelength regions of the spectrum. We

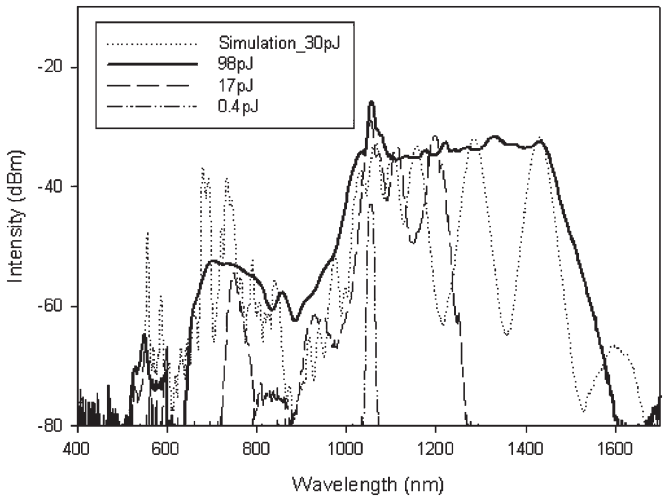

Fig. 7. Simulated and experimental optical spectra at the output of the SC-generation system for HF#1.

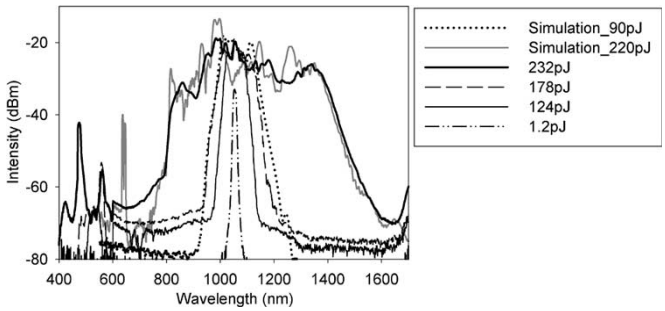

Fig. 8. Simulated and experimental optical spectra at the output of the SC-generation system for HF#2.

achieved a spectral broadening in excess of 1000 nm for launched pulse energies as low as $\sim$ 100 pJ. Note that we also investigated the sensitivity of the SC process to input pulse polarization but found the shape of the output SC spectrum to be relatively insensitive to this.

We next experimented with a short length ($\sim$ 6.8 cm) of Fiber#2 with a larger core diameter of $\sim$ 1.30 μm. In Fig. 8, we see that the SC-generation properties of this fiber are quite different from those of Fiber#1. Although the overall spectral broadening is not as strong (a bandwidth of $\sim$ 700 nm is observed in this case), broadening (at least up to certain power levels) occurred much more symmetrically than in Fiber#1. However, for pulse-energy levels higher than 178 pJ, spectral broadening was again more significant at longer rather than shorter wavelengths.

B. Numerical Model

We performed numerical simulations to help us interpret our SC-generation data. As with silica, we have assumed that SF57 glass is centrosymmetric and has a homogeneous third-order nonlinear susceptibility ($\chi^{(3)}$), which is small compared to the linear susceptibility, and is also wavelength independent over the wavelength range considered. The total refractive index therefore includes a small intensity-dependent nonlinear contribution ($n = n_0 + n_2 I$).

The model used to simulate pulse propagation includes both the instantaneous electronic response (responsible for the Kerr effect), and the delayed ionic response (responsible for Raman and Brillouin scattering) in the nonlinear component of the refractive index n_2. As is usual when modeling silica fibers, the nonlinear response to the applied field $A(z,t)$ has been written as $R(t) = (1 - f_{\mathrm{R}})\delta(t) + f_{\mathrm{R}}h(t)$, where the δ function represents the instantaneous electronic response, and $h(t)$ represents the delayed Raman response of the ions. The optical amplitude $A(z,t)$ will be changed according to

$$\Delta A(z,t) = i\gamma\left(1 + \frac{i}{\omega_0}\frac{\partial}{\partial t}\right) \times \left(A(z,t)\int_{-\infty}^{+t} R(t')\,|A(z,t-t')|^2\,dt'\right).$$

For silica, the Raman temporal response has been previously determined from the shape of the Raman gain in the frequency domain [18], and the Raman fraction of the total nonlinearity was determined to be 0.18 from measurements of the absolute value of the Raman gain. We are not aware of any previous measurements of the delayed temporal response or absolute Raman gain for SF57, and we have calculated the temporal response from uncalibrated spontaneous Raman spectra following the procedure used for silica by Stolen *et al.* [19]. For SF57, we assumed the Raman fraction of the total nonlinearity was $f_{\mathrm{R}} = 0.2$, based on the known fraction of 0.18 for silica. As far as we are aware, this is the first time that nonsilica Raman responses have been included in numerical SC simulations.

Effects such as two-photon absorption have not been included, and we have considered a single polarization only, and processes occurring within the fundamental fiber mode, and not mode mixing to possible higher order modes. These simplifications enable modeling of the pulse propagation using the modified nonlinear Schrödinger equation (NLSE) [20], with loss, as shown below, and as used previously for SC simulations [21]–[23]

$$\frac{\partial A}{\partial z} - i\sum_{k\geq 2}\frac{i^k\beta^k}{k!}\frac{\partial^k A}{\partial t^k} + \frac{\alpha(\omega)}{2}A = i\gamma\left(1 + \frac{i}{\omega_0}\frac{\partial}{\partial t}\right)\left(A(z,t)\int_{-\infty}^{+t} R(t')\,|A(z,t-t')|^2\,dt'\right)$$

where $A = A(z,t)$ is the electric field envelope, β_k are the dispersion coefficients at the center frequency ω_0, and $\alpha(\omega)$ is the frequency-dependent fiber loss. The full wavelength-dependent loss and dispersion profile of the fiber was included as shown in the previous sections. We used the A_{eff} data from the previous section as calculated at the seed-pulse wavelength. To solve the propagation equation, we used a standard split-step Fourier algorithm treating dispersion in the frequency domain and the nonlinearity in the time domain, apart from the temporal derivative for the self-steepening effect, which was evaluated using Fourier transforms. Our simulation results show the expected fine structuring [20], and we have applied a rolling average to smoothen the spectra, which should be approximately comparable to the time average over several pulses, which was measured in the experiments, and is computationally straightforward since it does not require repeated simulations with slight variations of the input pulse. We believe that, given the uncertainties of the exact characteristics of the fiber and the generally good agreement with the experimental data, the simulations provide a strong indication that the fiber performance may be understood based on the simulated dispersion profiles and nonlinearity. The simulated seed pulse was a transform-limited 300-fs [full-width at half-maximum (FWHM)] Gaussian profile at 1.055 μm.

C. Comparison of Simulations and Experimental Results

SC generation depends on the interplay between the seed pulse, fiber length, dispersion, nonlinearity, and loss. Considering the short lengths of fiber used in these experiments, we believe that the loss did not strongly influence the spectra, except possibly at wavelengths below $\sim$ 500 nm, where the absorption is strong. Furthermore, comparing fibers with different core sizes, the difference in nonlinearity parameter varied with effective mode area and, therefore, showed only a modest variation (Fig. 2). In addition, the width of the SC spectrum saturates after a threshold propagation distance along the fibers [23]. Therefore, the dispersion has the strongest influence on the shape of the continuum.

The 0.95-μm core fiber has a ZDW of $\sim$ 945 nm, so the dispersion is anomalous at the pump wavelength. Fig. 7 shows the experimental spectrum from the fiber, and there is clear evidence of the soliton-self-frequency shift (SSFS) transferring energy to longer wavelengths due to Raman gain, together with a dip in the spectrum close to the ZDW, and a low-power short-wavelength spectral peak. Comparing simulation results with the data, there is reasonable agreement with the overall shape of the spectra. Slight differences are that the short-wavelength peak is sharper in the simulation and that on the long-wavelength side, the individual Raman solitons have not merged to a flat continuum. We suggest that the flatter experimental spectrum may well be due to time averaging of several input pulses with a slight energy jitter, although we unfortunately did not measure the amplitude jitter of the launched pulses source during these experiments and are thus unable to substantiate this comment further. Furthermore, small differences between the simulated and the exact dispersion profile could change the position and shape of the short-wavelength peak and influence the soliton fission process, thus influencing the longer wavelength spectral shape. Such differences are to be expected since the calculated dispersion profiles shown in Fig. 3 are for fibers with core sizes in 0.1-μm increments, and a finer grid should enable closer agreement. We believe that the relatively high intensity at the pump wavelength in the experimental spectrum is due to some residual power guided along the cladding of this uncoated fiber, which, due to the larger cladding area, is not broadened by nonlinear effects.

The 1.30-μm core fiber has a ZDW of $\sim$ 1080 nm, so that the fiber has normal dispersion at the pump wavelength. The lower power spectra (both experimental and simulation plots) in Fig. 8 clearly show that a threshold power is required for

explosive spectral broadening. Simulations indicated that, for the first several centimeters of propagation, broadening was due to pure SPM in the normal-dispersion region and that only when sufficient power was transferred across the ZDW would soliton effect compression lead to SC. The propagation distance to the soliton effect compression reduced with increasing power from $\sim$ 7.5 cm at low power to $\sim$ 6.5 cm at high power. Therefore, for the experimental fiber length of 6.8 cm, the data in Fig. 8 show both behaviors were clearly observed. The high-power simulation spectrum shown in the figure is in good agreement with the experimental data and is reasonably flat from 800 to 1400 nm, apart from the dip close to the ZDW. We again interpreted differences between the simulation and experimental spectra to be due to slight differences between the calculated and actual dispersion profiles and to cladding guidance, leading to the increased experimentally measured intensity at the pump wavelength.

We also performed simulations for fibers with smaller core sizes than 0.95 μm which have increasing anomalous dispersion at the pump wavelength. Simulations for a 5-cm fiber length with 0.8-μm core diameter indicated that pulse energies of $\sim$ 100 pJ (as used in the above experiments) would produce a more pronounced blue-shifted component at $<$ 700 nm and Raman solitons extending to $>$ 1600 nm but with very low power in the range 700–900 nm (other authors have considered even smaller core sizes [16]). However, in practice, wavelengths below $\sim$ 500 nm would be strongly absorbed in longer lengths of SF57 fiber. Further simulations indicated that with $\sim$ 100-pJ pulses and 1.05-μm pump wavelength, the broadest and flattest continuum were produced by seeding slightly on the anomalous dispersion side of the ZDW, which corresponds to the dispersion profiles of fibers with core sizes in the range 1.0–1.1 μm. The predicted spectra spanned from 750 to 1500 nm. Fibers with core sizes above 1.4 μm were not predicted to be efficient for continuum generation due to the strong normal dispersion at the pump wavelength.

For all of the fibers, the steep dispersion profile at short wavelengths was due to the need for a large waveguide dispersion to shift the bulk SF57 ZDW from $\sim$ 1.97 μm towards the $\sim$ 1.05-μm pump wavelength. The steep dispersion prevented broad visible continuum generation with this pump wavelength. To create an SF57 fiber with a flatter dispersion profile would require moving the fiber ZDW closer to that of the bulk glass, e.g., a dispersion-flattened SF57 HF with $\sim 1.5-1.6$-μm ZDW is likely to be feasible [25] (for comparison, the ZDW of bulk silica is at 1.3 μm, and therefore, a smaller waveguide dispersion is required to shift the ZDW to 1 μm, and, as a consequence, a dispersion-flattened silica HF with ZDW at 1 μm is feasible). Since an SC source comprises both a nonlinear fiber and pump laser, we expect that a dispersion-flattened SF57 HF with an Er-fiber pump system could provide a very attractive and practical source for broadband continuum generation in the 1–2-μm-wavelength region.

V. Conclusion

We have used extrusion techniques to fabricate small-core HFs with an extremely high effective nonlinearity in lead-silicate glass (SF57). The fibers we have fabricated exhibit an effective nonlinearity of 1860 $\mathrm{W}^{-1} \cdot \mathrm{km}^{-1}$, which is the highest value reported to date for a fiber at 1550 nm. By carefully tailoring the size of the microstructure, we achieved a ZDW of $\sim$ 1 μm, which made our fibers extremely useful for SC-generation applications at that wavelength. We have used two HFs that differed only slightly in the size of their cores to demonstrate the critical effect of dispersion in the SC-generation process. We backed our experimental findings with numerical simulations of the SC generation, which enabled us to explain fully the nonlinear behavior of the HFs.

This paper highlights the potential of this technology and material for nonlinear applications. We believe that similar techniques can be applied at longer wavelengths as well, which are better suited to the material dispersion of this glass, e.g., for SC generation extending beyond 2 μm.

Acknowledgment

The authors would like to thank R. Paschotta of RP Photonics Consulting for providing the software for pulse propagation modeling.

References

[1] J. C. Knight, T. A. Birks, P. S. J. Russell, and D. M. Atkin, "All-silica single-mode photonic crystal fiber," *Opt. Lett.*, vol. 21, no. 19, pp. 1547–1549, Oct. 1996.

[2] T. M. Monro and D. J. Richardson, "Holey optical fibres: Fundamental properties and device applications," *Comptes Rendus Physique*, vol. 4, no. 1, pp. 175–186, Jan. 2003.

[3] J. H. Lee, W. Belardi, K. Furusawa, P. Petropoulos, Z. Yusoff, T. M. Monro, and D. J. Richardson, "Four-wave mixing based 10-Gb/s tunable wavelength conversion using a holey fiber with a high SBS threshold," *IEEE Photon. Technol. Lett.*, vol. 15, no. 3, pp. 440–442, Mar. 2003.

[4] V. Finazzi, T. M. Monro, and D. J. Richardson, "Small-core silica holey fibers: Nonlinearity and confinement loss trade-offs," *J. Opt. Soc. Amer. B, Opt. Phys.*, vol. 20, no. 7, pp. 1427–1436, Jul. 2003.

[5] T. M. Monro, Y. D. West, D. W. Hewak, N. G. R. Broderick, and D. J. Richardson, "Chalcogenide holey fibers," *Electron. Lett.*, vol. 36, no. 24, pp. 1998–2000, Nov. 2000.

[6] V. Kumar, A. K. George, J. C. Knight, and P. S. Russell, "Tellurite photonic crystal fiber," *Opt. Express*, vol. 11, no. 20, pp. 2641–2645, Oct. 2003.

[7] A. Mori, K. Shikano, W. Enbutsu, K. Oikawa, K. Naganuma, M. Kato, and S. Aozasa, "1.5 μm band zero-dispersion shifted tellurite photonic crystal fibre with a nonlinear coefficient of 675 $\mathrm{W}^{-1}\mathrm{km}^{-1}$," presented at the Eur. Conf. Optical Communication (ECOC), Stockholm, Sweden, Sep. 5–9, 2004, Paper Th3.3.6.

[8] H. Ebendorff-Heidepriem, P. Petropoulos, S. Asimakis, V. Finazzi, R. C. Moore, K. Frampton, F. Koizumi, D. J. Richardson, and T. M. Monro, "Bismuth glass holey fibers with high nonlinearity," *Opt. Express*, vol. 12, no. 21, pp. 5082–5087, Oct. 2004.

[9] K. M. Kiang, K. Frampton, T. M. Monro, R. Moore, J. Tucknott, D. W. Hewak, D. J. Richardson, and H. N. Rutt, "Extruded single-mode non-silica glass holey optical fibres," *Electron. Lett.*, vol. 38, no. 12, pp. 546–547, Jun. 2002.

[10] V. V. R. K. Kumar, A. K. George, W. H. Reeves, J. C. Knight, P. S. J. Russell, F. G. Omenetto, and A. J. Taylor, "Extruded soft glass photonic crystal fiber for ultrabroad supercontinuum generation," *Opt. Express*, vol. 10, no. 25, pp. 1520–1525, Dec. 2002.

[11] P. Petropoulos, T. M. Monro, H. Ebendorff-Heidepriem, K. Frampton, R. C. Moore, and D. J. Richardson, "Highly nonlinear and anomalously dispersive lead silicate glass holey fibers," *Opt. Express*, vol. 11, no. 26, pp. 3568–3573, Dec. 2003.

[12] J. Y. Y. Leong, P. Petropoulous, S. Asimakis, H. Ebendorff-Heiderpriem, R. C. Moore, K. Frampton, V. Finazzi, X. Feng, J. H. V. Price, T. M. Monro, and D. J. Richardson, "A lead silicate holey fiber with $\gamma = 1860\ \mathrm{W}^{-1}\mathrm{km}^{-1}$ at 1550 nm," presented at the Optical Fiber Communication (OFC), Anaheim, CA, 2005, PDP22.

[13] E. M. Vogel, M. J. Weber, and D. M. Krol, "Nonlinear optical phenomena in glass," *Phys. Chem. Glasses*, vol. 32, no. 6, pp. 231–254, 1991.
[14] *Schott E-Catalogue 2003 Optical Glass, Schott Glass, Mainz, Germany*. [Online]. Available: http://www.schott.com/optics_devices/english/download/catalog_optical_glass_informations_2003.pdf
[15] J. C. Knight, J. Arriaga, T. A. Birks, A. Ortigosa-Blanch, W. J. Wadsworth, and P. S. J. Russell, "Anomalous dispersion in photonic crystal fiber," *IEEE Photon. Technol. Lett.*, vol. 12, no. 7, pp. 807–809, Jul. 2000.
[16] A. V. Husakou and J. Herrmann, "Supercontinuum generation in photonic crystal fibers made from highly nonlinear glasses," *Appl. Phys., B Lasers Opt.*, vol. 77, no. 2/3, pp. 227–234, Sep. 2003.
[17] A. Boskovich, S. V. Chernikov, J. R. Taylor, L. Gruner-Nielsen, and O. A. Levring, "Direct continuous-wave measurement of n_2 in various types of telecommunication fiber at 1.55 μm," *Opt. Lett.*, vol. 21, no. 24, pp. 1966–1968, Dec. 1996.
[18] R. H. Stolen, C. Lee, and R. K. Jain, "Development of the stimulated Raman-spectrum in single-mode silica fibers," *J. Opt. Soc. Amer. B, Opt. Phys.*, vol. 1, no. 4, pp. 652–657, Aug. 1984.
[19] R. H. Stolen, J. P. Gordon, W. J. Tomlinson, and H. A. Haus, "Raman response function of silica-core fibers," *J. Opt. Soc. Amer. B, Opt. Phys.*, vol. 6, no. 6, pp. 1159–1166, Jun. 1989.
[20] G. P. Agrawal, *Nonlinear Fiber Optics*. San Diego, CA: Academic, 1995.
[21] J. H. Price, T. M. Monro, K. Furusawa, W. Belardi, J. C. Baggett, S. J. Coyle, C. Netti, J. J. Baumberg, R. Paschotta, and D. J. Richardson, "UV generation in a pure silica holey fiber," *Appl. Phys., B Lasers Opt.*, vol. 77, no. 2/3, pp. 291–298, Sep. 2003.
[22] J. M. Dudley and S. Coen, "Coherence properties of supercontinuum spectra generated in photonic crystal and tapered optical fibers," *Opt. Lett.*, vol. 27, no. 13, pp. 1180–1182, Jul. 2002.
[23] G. Genty, M. Lehtonen, H. Ludvigsen, J. Broeng, and M. Kaivola, "Spectral broadening of femtosecond pulses into continuum radiation in microstructured fibers," *Opt. Express*, vol. 10, no. 20, pp. 1083–1098, Oct. 2002.
[24] G. Q. Chang, T. B. Norris, and H. G. Winful, "Optimization of supercontinuum generation in photonic crystal fibers for pulse compression," *Opt. Lett.*, vol. 28, no. 7, pp. 546–548, Apr. 2003.
[25] J. Y. Y. Leong, S. Asimakis, F. Poletti, P. Petropoulos, X. Feng, R. C. Moore, K. E. Frampton, T. M. Monro, H. Ebendorff-Heiderpriem, W. H. Loh, and D. J. Richardson, "Towards zero dispersion highly nonlinear lead silicate glass holey fibres at 1550 nm by structured-element-stacking," presented at the Eur. Conf. Optical Communication (ECOC), Glasgow, U.K., 2005, Th4.4.5 (Postdeadline).

J. Y. Y. Leong was born in Malaysia in 1978. She received the B.Sc. (Hons.) in electrical and electronic engineering (first-class honors) in 2001 from The University of Technology, Malaysia. In 2001, she received a scholarship from The Ministry of Science, Technology, and Environment (MOSTE) of the Malaysian Government to pursue the doctorate degree under the supervision of Prof. D. Richardson. Currently, she is working towards the Ph.D. degree in optoelectronics with particular emphasis on design and fabrication of highly nonlinear nonsilica photonics crystal fibers at the University of Southampton, Southampton, U.K.

P. Petropoulos was born in Patras, Greece. He graduated from the Department of Electrical Engineering and Information Technology, University of Patras, in 1995, received the M.Sc. degree in communications engineering from the University of Manchester Institute of Science and Technology, Manchester, U.K., in 1996, and the Ph.D. degree in optical telecommunications from the Optoelectronics Research Centre (ORC), University of Southampton, Southampton, U.K. in 2000.

His research interests include all-optical processing and switching in optical fibers; pulse manipulation for optical communications using fiber Bragg gratings, including applications in optical correlation systems for the implementation of optical code division multiple access and optical packet switched systems; silica and compound glass holey fibers and their nonlinear applications; and fiber lasers. His research has produced more than 100 papers in journals and conferences in the field of optical physics and optical communications. He is currently a Southampton Senior Research Fellow at the ORC.

J. H. V. Price received the B.A.(Hons.) in physics from Oxford University, Oxford, U.K., in 1991, the Masters of Engineering Science degree from Cornell University, Ithaca, NY, in 2000, and the Ph.D. degree in electronics and computer science from the University of Southampton, Southampton, U.K., in 2003.

He is currently a Research Fellow with the Physics and Astronomy/Optoelectronics Research Centre. His research is developing high power, femtosecond, pulsed-fiber laser sources. The systems are based on Ytterbium doped fiber, operating at wavelengths close to 1 μm.

Heike Ebendorff-Heidepriem, photograph and biography not available at the time of publication.

S. Asimakis received the degree from the Department of Physics, Aristotle University of Thessaloniki, Greece, in 2001 and the M.Sc. degree in communication systems and signal processing from the University of Bristol, Bristol, U.K., in 2002. He joined the Optical Research Center, University of Southampton, Southampton, U.K., in January 2004 to pursue the Ph.D. degree in optical communications. His Ph.D. studies are financially supported by the Greek State Scholarships Foundation (I.K.Y).

His main research interests focus on microstructured fibres and nonlinear optics.

R. C. Moore, photograph and biography not available at the time of publication.

K. E. Frampton, photograph and biography not available at the time of publication.

V. Finazzi, photograph and biography not available at the time of publication.

X. Feng received the Doctor of Engineering degree in material science from the Shanghai Institute of Optics and Fine Mechanics, Chinese Academy of Sciences, Shanghai, China, in 1999.

He joined the soft-glass group of the Optoelectronics Research Centre, University of Southampton, Southampton, U.K., in 2001. He was a post-doctoral researcher with Kyoto University, Kyoto, Japan, and Rutgers, The State University of New Jersey, New Brunswick. His current research interests include the fabrication and the applications of microstructured speciality optical fibers based on nonsilica optical glasses.

T. M. Monro, photograph and biography not available at the time of publication.

D. J. Richardson was born in Southampton, U.K., in 1964. He received the B.Sc. degree and the Ph.D. degree in fundamental physics from Sussex University, U.K., in 1985 and 1989, respectively.

In May 1989, he was a Research Fellow at the then recently formed Optoelectronics Research Centre (ORC), Southampton University, U.K. He is currently a Deputy Director at the ORC, responsible for much of the ORC's fiber-related activities. He is one of the founders of Southampton Photonics Incorporated, a university spin-off venture that has successfully commercialized elements of high-power laser technology developed within the ORC. His current research interests include amongst others: holey fibers, high-power fiber lasers, short pulse lasers, optical fiber communications, all-optical processing and switching, nonlinear optics, and the physics and applications of microstructured nonlinear/linear media. He has published more than 400 conference and journal papers in his 15 years at the ORC and produced over 15 patents.

Prof. Richardson is a frequent Invited Speaker at leading international optics conferences in the optical communications, laser, and nonlinear optics fields, and an active member of both the national and international optics communities. He was awarded a Royal Society University Fellowship in 1991 in recognition of his pioneering work on short-pulsed fiber lasers.